Chapter 7

Free Shear Flows

Javier Jiménez
School of Aeronautics
Universidad Politécnica de Madrid

Summary

This chapter and the next one describe particular classes of turbulent flows. The present one deals with incompressible constant-density flows away from walls, which include shear layers, jets and wakes behind bodies. It can be divided into two parts. The first one is a phenomenological description of those flows, including their theoretical treatment as far as it can be carried without worrying about the details of the flow structure. The second part deals with structure, and leads us into an elementary discussion of hydrodynamic stability, of rapid-distortion theory, and of their relation with the dynamics of the large flow scales. This second part also describes some of the technological applications of free shear flows, and how our understanding of their dynamics allows us to develop strategies for their control. Most of the chapter uses the plane free shear layer as a characteristic example, but the same ideas can be extended, with suitable modifications, to other flows in this class.

This and the following chapter are reference material. They are self-contained in the sense that the flows described in the present chapter can be understood relatively independently of the wall-bounded ones described in the next one, and viceversa. They are applications to the real world of the theory that has been developed up to now, and an effort has been made to include in them as much as possible of the theoretical and experimental information on the flows under discussion. As we have seen in the previous chapters, structures below the Corrsin scale are approximately the same in all turbulent flows. The discussion in these two chapters deals therefore mostly with the large scales which depend on the energy-injection mechanism.

7.1 The plane free shear layer

The plane shear layer is the classical example of a turbulent shear flow away from walls. Two parallel streams of different velocities are separated by a thin plate and come together

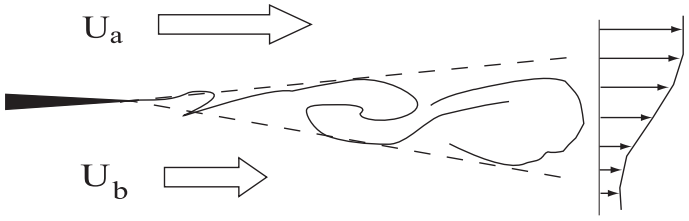

FIGURE 7.1. Sketch of a plane shear layer.

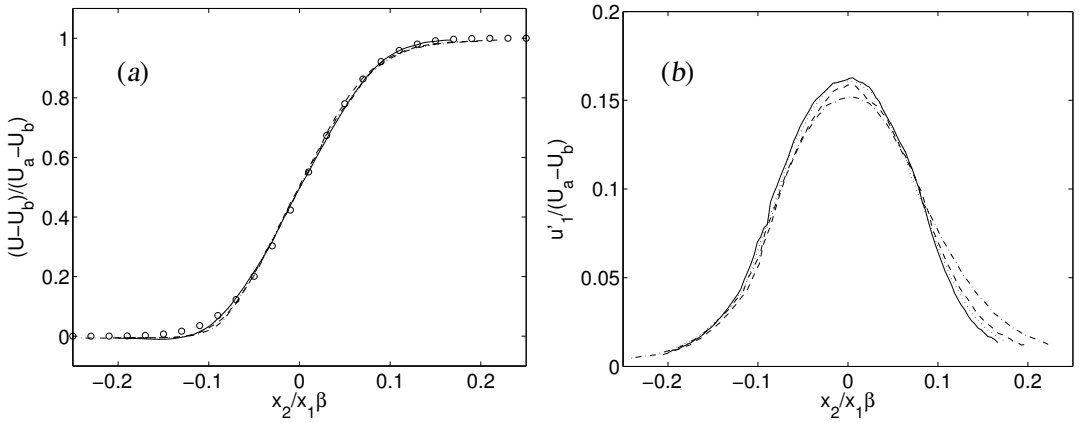

FIGURE 7.2. Plane shear layer. (*a*) Mean streamwise velocity, (*b*) Root mean square streamwise velocity. $\beta = 0.3$, $\Delta U\theta_0/\nu = 2900$, where θ_0 is the initial momentum thickness. —·— , $\beta x_1/\theta_0 = 40$; - - - - , 60; ····· , 90; ——— , 135, from Delville, Bellin & Bonnet (1988); ∘ in (*a*) is the constant eddy viscosity approximation (7.18).

as the plate ends. The layer grows from the resulting velocity discontinuity and thickens downstream (figure 7.1). Shear layers appear within many other flows, such as in the initial part of jets, and on top of locally-separated boundary layers. They are technologically important because they generate noise and dissipate energy, and are therefore a source of drag, but also because, if the two streams contain different fluids, it is in the shear layer that the mixing occurs. Most industrial combustors, and many of the mixers in chemical industry, are designed around shear layers. It is probably because of this that they were one of the first turbulent flows to be understood in detail, and also one of the first to be controlled.

A lot can be said about the shear (or mixing) layer from dimensional considerations. An ideal layer grows from a discontinuity of zero thickness and, if viscosity can be neglected, has no length scale except for the distance to the origin. The only other parameters are the velocities of the two free streams, $U_a > U_b$. The mean velocity, or the r.m.s. fluctuations, must therefore take the form

$$\frac{U(x_2)}{\Delta U},\ \frac{u'}{\Delta U},\ \ldots = f(x_2/x_1,\ \beta) \tag{7.1}$$

where $\Delta U = U_a - U_b$ is the velocity difference between the streams, $U_c = (U_b + U_a)/2$ is the mean velocity, and $\beta = \Delta U/2U_c$ is a parameter characterizing the velocity ratio. The

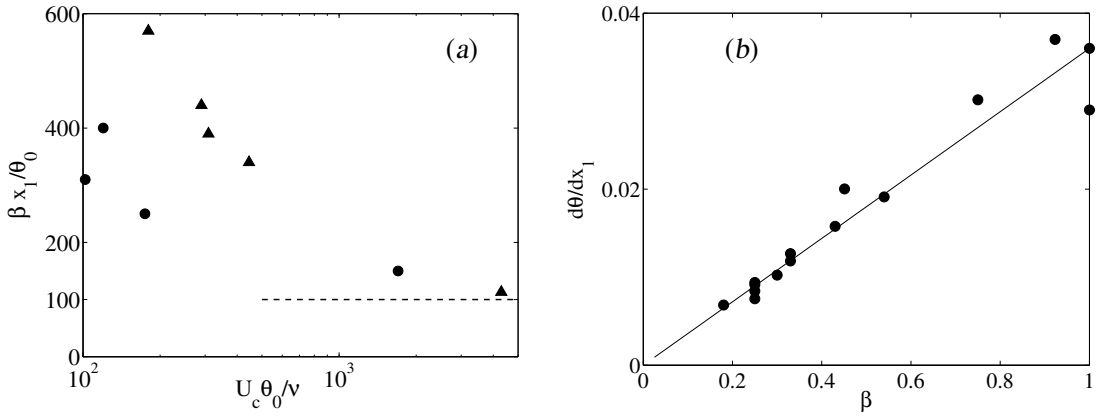

FIGURE 7.3. (*a*) Location in which the velocity fluctuations in a plane shear layer become self-similar, as a function of the initial boundary-layer Reynolds number. Data from various experimenters and at different β. • , initially laminar boundary layers; ▲ , tripped or turbulent ones. Adapted and augmented from Hussain & Zedan (1978). (*b*) Growth rate of experimental shear layers, from various sources. The solid line is $\mathrm{d}\theta/\,\mathrm{d}x_1 = 0.036\beta$.

streamwise and transverse coordinates are x_1 and x_2. Figure 7.2 shows that the similarity law (7.1) is approximately satisfied by experiments.

In real flows the thickness of the boundary layers on both sides of the splitter plate provides a length scale for the initial development of the mixing region, and similarity laws such as (7.1) only hold some distance downstream from the origin. A useful definition is the momentum thickness,

$$\theta = \int_{-\infty}^{\infty} \frac{U - U_b}{\Delta U}\left(1 - \frac{U - U_b}{\Delta U}\right)\mathrm{d}x_2, \tag{7.2}$$

which is related to the momentum deficit with respect to a sharp discontinuity, but which can be understood most easily as being the simplest integral expression of the mean velocity which remains integrable at $x_2 \to \pm\infty$. The self-similar behaviour in shear layers is typically achieved at distances from the plate of the order of a few hundred initial momentum thicknesses, θ_0, although the precise value depends on the Reynolds number and on the details of the initial boundary layers. We will see below that the proper dimensionless parameter for the onset of similarity is $\beta x_1/\theta_0$, which is related to the preferred wavelength of the initial instability of the shear-layer profile. Experimental data are summarized in figure 7.3(*a*). The asymptotic value, $\beta x_1/\theta_0 \approx 100$, is achieved when the initial Reynolds number is $Re_0 = U_c\theta_0/\nu \gtrsim 1000$.

To account for this initial development of the shear layer the origin of coordinates in (7.1) has to taken some distance x_0 from the end of the splitter plate. The magnitude, and even the sign, of this offset depends on the initial boundary layers, but decreases as the initial Reynolds number increases. For $Re_0 \gtrsim 1000$, $\beta x_0/\theta_0 \approx 10 - 20$, upstream of the edge of the splitter plate.

It follows from the small values of x_2/x_1 in figure 7.2 that the layer spreads slowly. This is a common property of shear flows, which could have been anticipated when we saw in §5.4 that turbulent dissipation is a weak process. The turbulent region cannot spread

without dissipating energy, and the result is that the flow is slender, much longer than it is wide. Consider for example a shear layer with the simplified velocity profile

$$U = \begin{cases} U_a & \text{if} \quad x_2 \geq \delta/2 \\ U_c + \Delta U x_2/\delta & \text{if} \quad |x_2| < \delta/2 \\ U_b & \text{if} \quad x_2 \leq -\delta/2 \end{cases} \tag{7.3}$$

where the thickness of the layer, $\delta(x_1)$, varies downstream. The energy flux across a plane normal to the mean flow, extending from $x_2 = -H$ to $x_2 = H \gg \delta$, and of unit spanwise width, is

$$\Phi = \int_{-H}^{H} \rho \frac{U^3}{2} \mathrm{d}x_2 = \rho \frac{U_a^3 + U_b^3}{2} H - \rho U_c^3 \beta^2 \delta. \tag{7.4}$$

As the layer thickens downstream, the decrease of this energy flux has to be compensated by the energy dissipation over the turbulent volume

$$\frac{\mathrm{d}\Phi}{\mathrm{d}x_1} = -\rho U_c^3 \beta^2 \frac{\mathrm{d}\delta}{\mathrm{d}x_1} = -\rho \varepsilon \delta. \tag{7.5}$$

We can estimate ε from the properties of the largest turbulent eddies, which have to be of size $O(\delta)$, and which have characteristic velocities of the order of $u_\delta \approx \Delta U/2$ to accommodate the velocity difference between the two streams. Using (5.45) we obtain

$$\varepsilon \approx 0.1 \frac{u_\delta^3}{\delta} \approx 0.1 U_c^3 \beta^3, \tag{7.6}$$

and finally,

$$\frac{\mathrm{d}\delta}{\mathrm{d}x_1} \approx 0.1\beta. \tag{7.7}$$

Since $0 \leq \beta \leq 1$ whenever the two streams are co-flowing, the growth of the layer is always slow.

Problem 7.1: Show that the momentum thickness for the velocity profile (7.3) is $\theta = \delta/6$.

The slow growth allows free shear flows to be approximated as quasi-parallel, and leads to another derivation of (7.7) which is often more useful than the previous one. For shear layers, for example, we can think of the flow as spreading laterally while being advected downstream with a mean velocity U_c. The underlying approximation is that the dynamics of the turbulence, such as for example the determination of the energy dissipation rate, is associated with scales of $O(\delta)$, and that the relative change of the thickness of the layer in those distances is $\delta^{-1}(\,\mathrm{d}\delta/\,\mathrm{d}x_1\,\delta) \ll 1$. The downstream coordinate can thus be converted to an evolution time $t = x_1/U_c$ and, in that moving frame of reference, the only velocity scale is the difference ΔU. The lateral spreading rate must then be proportional to

$$\frac{\mathrm{d}\theta}{\mathrm{d}x_1} \approx \frac{1}{U_c} \frac{\mathrm{d}\theta}{\mathrm{d}t} = C_L \frac{U_a - U_b}{U_a + U_b}. \tag{7.8}$$

This and the previous energy-budget analysis are only approximations, but the prediction that the spreading rate should be proportional to β is well satisfied (figure 7.3*b*), with $C_L \approx$

$0.035 - 0.045$. A formal justification of the approximation leading to (7.8) can be found in problem 7.2

The shape of the profile is also well represented by a crude eddy-viscosity approximation. Assume an eddy viscosity which is constant across the layer and that, on dimensional grounds, has the form

$$\nu_\varepsilon = C' \Delta U \theta. \tag{7.9}$$

Neglecting longitudinal gradients and transforming the problem to a temporal one in the advective frame of reference, the mean velocity satisfies a diffusion equation whose solution is an error function [PROBLEM 7.2]. It agrees quantitatively with the measured velocity profiles if $C' \approx 0.063$ (figure 7.2*a*). The 'Reynolds number' of the turbulent shear layer, based on its momentum thickness, on the velocity difference, and on that eddy viscosity, is about 15, which is of the same order as the effective Reynolds numbers obtained in §5.4. Note that this value is independent of the actual molecular Reynolds number, underscoring again that molecular viscosity is negligible for the large scales of turbulent flows, and therefore for the Reynolds stresses and for the velocity profile.

Problem 7.2: The boundary layer approximation. Write the approximate equation for a slowly growing free shear layer. Justify the limit in which the mean advection approximation (7.8) holds, integrate the resulting equation, using the uniform eddy viscosity model (7.9), and relate its proportionality constant C' to the growth rate C_L of the momentum thickness.

Solution: The slow-growth approximation means that streamwise dimensions are much longer than transverse ones, so that streamwise derivatives of similar quantities can be neglected with respect to transverse ones. Such simplifications are often the key to solving problems in fluid mechanics, which are otherwise too complex to allow simple solutions. It is important to gain some familiarity with them.

Assume that the ratio of x_2 to x_1 is of the order of a small quantity $\epsilon \ll 1$. The continuity equation for the longitudinal and transverse mean velocities, U and V, is

$$\partial_1 U + \partial_2 V = 0, \tag{7.10}$$

which, since $\partial_1 = O(\epsilon \partial_2)$, implies that $V = O(\epsilon U)$. Choose units such that ∂_2 is $O(1/\epsilon)$ and V is $O(\epsilon)$, while U and and ∂_1 are $O(1)$. This implies that $x_2 = O(\epsilon)$ and $x_1 = O(1)$. The two mean momentum equations are

$$U\partial_1 U + V\partial_2 U + \partial_1 p = \partial_1(\nu_\varepsilon \partial_1 U) + \partial_2(\nu_\varepsilon \partial_2 U), \tag{7.11}$$

and

$$U\partial_1 V + V\partial_2 V + \partial_2 p = \partial_1(\nu_\varepsilon \partial_1 V) + \partial_2(\nu_\varepsilon \partial_2 V). \tag{7.12}$$

In both equations the longitudinal derivatives in the right-hand sides are $O(\epsilon^2)$ with respect to the transverse ones, and can be neglected. In the transverse momentum equation (7.12) the first two terms are $O(\epsilon)$, and the equation reduces to $p = O(\nu_\varepsilon)$. When this is substituted in (7.11), the pressure gradient is seen to be of order $\partial_1 p = O(\nu_\varepsilon)$, and can be neglected when compared with the Reynolds stresses in the right-hand side, which are $O(\nu_\varepsilon/\epsilon^2)$. The simplified streamwise-momentum equation is then

$$U\partial_1 U + V\partial_2 U = \partial_2(\nu_\varepsilon \partial_2 U), \tag{7.13}$$

in which all the terms in the left-hand side are $O(1)$, while the one in the right-hand side is $O(\nu_\varepsilon/\epsilon^2)$. This shows that the condition for the spreading rate to be slow is that the eddy viscosity also has to be small, $\nu_\varepsilon = O(\epsilon^2)$, and anticipates that the proportionality constant C' in (7.9) will be found to be $O(\epsilon)$.

Equation (7.13) has to be solved together with the continuity equation (7.10) and the two constitutive equations (7.8) and (7.9). We can remove most of the parameters by defining new variables

$$U = U_c + \Delta U u, \qquad x_2 = \epsilon x_2', \qquad V = \epsilon \Delta U v, \tag{7.14}$$

where $\epsilon = (2C_L C')^{1/2}\beta$. This change of variables implements the scalings discussed above, and leaves the continuity equation invariant. The momentum equation becomes

$$\partial_1 u + 2\beta(u\partial_1 u + v\partial_2' u) = \partial_2'(x_1\partial_2' u), \tag{7.15}$$

where $\partial_2' = \partial/\partial x_2'$. This equation is still complicated, and only simplifies when $\beta \ll 1$. The limit in which terms of $O(\beta)$ are neglected is the mean advection approximation discussed in (7.8), since x_1 can then be treated as a time, and the shear layer grows thicker as the 'time' increases downstream. The final simplified equation is

$$\partial_1 u = \partial_2'(x_1\partial_2' u). \tag{7.16}$$

The boundary conditions are that $u = \pm 1/2$ when $x_2 \to \pm\infty$. The problem is initialized at $x_1 = 0$ with a velocity discontinuity in which $u = 1/2$ if $x_2 > 0$, and $u = -1/2$ otherwise. There is no length scale in this problem, as seen from the property that (7.16) is not changed by rescaling x_1 and x_2' by a common factor, and the solution can be expected to depend only on the dimensionless group $\xi = x_2'/x_1$. The equation satisfied by this *similarity* solution is found by substitution to be

$$\xi\partial_\xi u + \partial_{\xi\xi} u = 0, \tag{7.17}$$

which can be integrated directly to

$$u = \frac{1}{2}\,\mathrm{erf}(\xi/\sqrt{2}). \tag{7.18}$$

Using this solution in the definition (7.2) of the momentum thickness, and transforming back into dimensional variables, we finally obtain,

$$\theta = \int_{-\infty}^{\infty}\left(\frac{1}{4} - u^2\right)\mathrm{d}x_2 = \epsilon x_1 \int_{-\infty}^{\infty}\left(\frac{1}{4} - u^2\right)\mathrm{d}\xi \approx 0.798(C'C_L)^{1/2}\beta x_1. \tag{7.19}$$

When this is compared with the experimental growth law (7.8), it provides a relation between the experimental results and the empirical modelling coefficient,

$$C' \approx 1.57 C_L, \tag{7.20}$$

which is the one used in the text and in figure 7.2(*a*). Although the numerical value for C_L has to be obtained from experiments in this simplified model, the form (7.18) is a prediction which does not depend on the adjustable parameter C', and which agrees well with the experimental profiles even if the value of $\beta\,(= 0.3)$ is not very small. We also can check at this stage whether the original boundary layer approximation, which required that $\epsilon \ll 1$, was justified. It follows from (7.20), and from the experimental value $C_L \approx 0.04$, that

$$\epsilon = (2C_L C')^{1/2}\beta \approx 0.07\,\beta, \tag{7.21}$$

which is small for any value of β. The full equation (7.15) also admits a similarity solution depending only of ξ. The dependence of the growth rate on β is in that case not as simple as (7.8), but the difference between the growth rates deriving from both approximations is, in practice, small.

7.2 The large-scale structures

Given the success of the crude approximations used in the previous section, which essentially substitute turbulence by a homogeneous fluid with a modified viscosity, it was a surprise to find that the largest scales of the plane shear layer were anything but homogeneous, and that the flow could be understood, in large part, in terms of linear stability theory.

The key observation was made by Brown & Roshko (1974), although indications had been accumulating for several years. They found that the interface between the two streams takes the form of large, organized, quasi-two-dimensional structures, which span essentially the whole width of the layer (figure 7.4.*a*). Those structures are strikingly reminiscent of the linear instabilities of a smoothed velocity discontinuity, which we already discussed in

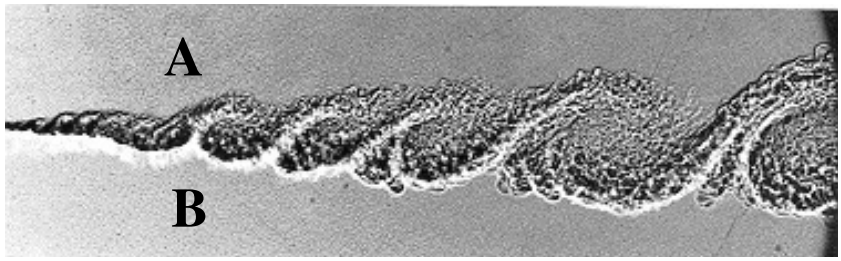

(*a*)

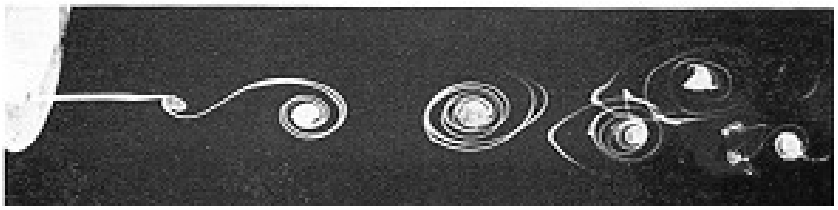

(*b*)

FIGURE 7.4. (*a*) Turbulent shear layer at high Reynolds number between two streams of different gases (Brown & Roshko 1974). The Reynolds number based on the velocity difference and on the maximum visual thickness is $Re \approx 2 \times 10^5$. (*b*) Initial development of a low Reynolds number velocity discontinuity (Freymuth 1966). $Re \approx 7,500$.

chapter 2 as the Kelvin–Helmholtz instability of a two-dimensional vorticity layer. It will moreover be shown below that not only the shape of the structures, but their wavelengths and internal organization, agree remarkably well with two-dimensional stability results which one would only expect to apply to laminar mixing layers (figure 7.4.*b*).

We have invoked flow instabilities several times in the previous chapters, but never discussed them in detail. Hydrodynamic stability is similar to that of other mechanical systems. Small perturbations to stable equilibrium states remain small, and die in the presence of friction. Unstable perturbations grow until the system moves far from its original state. The concept can be extended to more complicated dynamical structures, such as periodic orbits or complex attractors, but needs some qualification when applied to turbulent flows. Since the basic flow is not steady, the instabilities have to compete with other flow processes to be able to grow, and only those with sufficiently fast growth rates are relevant.

Flow instabilities are studied by linearizing the equations of motion about some mean equilibrium solution. The procedure is similar to the Reynolds decomposition introduced in §5.3, but the perturbations are assumed to be small, and all the quadratic terms are neglected, including the Reynolds stresses.

That linear processes might be important in turbulence should not be a surprise. We have already seen that turbulence is in general a weak phenomenon. The velocity fluctuations in figure 7.2(*b*), for example, are small compared with the velocity difference between the two streams. If we assume that there are structures of the size of the shear layer thickness, θ, their internal deformation times would be of the order θ/u', while the shearing time due to the mean flow, $\theta/\Delta U$, would be shorter. The shortest time controls the dynamics of the flow, and the large scales are controlled by the linear processes due to the mean flow, instead of by their nonlinear self-deformation. This was the essence of the argument in §5.3 that, in the presence of shear, the structures larger than the Corrsin scale interact directly

with the shear to extract energy from it. Those large scales are essentially linear, but the internal times of the turbulent eddies decrease with their size, and any linear process that we may identify as being important for the larger flow scales does not necessarily remain relevant for the smaller ones below the Corrsin scale.

The characteristic property of free shear flows is that the linear dynamics of their large scales is unstable.

7.2.1 *Linear processes in turbulence*

Consider a base flow $\boldsymbol{U}(\boldsymbol{x},\, t)$, satisfying the equations of motion, on which infinitesimal fluctuations $\widetilde{u}$ are superimposed. Neglecting terms of order $\widetilde{u}^2$, the evolution equations for the fluctuations are

$$\partial_t \widetilde{u}_k + U_j \partial_j \widetilde{u}_k + \widetilde{u}_j \partial_j U_k + \partial_k \widetilde{p} = \nu \nabla^2 \widetilde{u}_k, \tag{7.22}$$

$$\partial_k \widetilde{u}_k = 0. \tag{7.23}$$

Note that, even if we neglect the quadratic Reynolds stresses in the momentum equation, an energy equation similar to (5.40) can be obtained by contracting (7.22) with $\widetilde{u}_k$, and that it contains a production term, $\widetilde{u}_k \widetilde{u}_j \partial_j U_k$, which is identical to (5.43). The linearized fluctuations can extract energy from the mean flow through this term, or lose it, and as a consequence they can grow or decay in times scales which are governed by the mean velocity gradient. The only simplification that linearization brings to the energy equation is the disappearance of the cubic terms from the energy flux (5.41). Flows governed by the linearized equations (7.22)–(7.23) are said to follow 'rapid distortion theory' (RDT), because the distortion induced by the base flow is fast compared with the self-deformation produced by the fluctuations themselves.

As in all incompressible flows the pressure can be eliminated from (7.22) by invoking continuity. Taking the divergence of (7.22) and using the incompressibility both of the fluctuations and of the base flow we obtain

$$\nabla^2 \widetilde{p} = -2(\partial_k U_j)(\partial_j \widetilde{u}_k). \tag{7.24}$$

A particularly case in which the results of the linear approximation can be analysed fairly easily is when the velocity gradient tensor of the base flow varies smoothly enough to be considered as constant over the length scales of the fluctuations, and can be approximated as being only a function of time. The coefficients of the resulting RDT equations do not contain $\boldsymbol{x}$ explicitly, and the solutions can be expanded in terms of elementary Fourier functions,

$$\widetilde{u}_k = \widehat{u}_k \exp(\mathrm{i}\kappa_j x_j), \tag{7.25}$$

with a similar expansion for $\widetilde{p}$. The solution to Poisson's equation (7.24) is then

$$\widehat{p} = 2\mathrm{i}(\partial_k U_j)\kappa_j \widehat{u}_k / |\kappa|^2, \tag{7.26}$$

where $|\kappa|^2 = \kappa_j \kappa_j$, and can be substituted into (7.22). The resulting evolution equations can only be satisfied if both the amplitudes $\widehat{u}_k$ and the wavenumbers κ_j are functions of time satisfying

$$\partial_t \widehat{u}_k = -\left(\delta_{jk} - 2\frac{\kappa_j \kappa_k}{|\kappa|^2}\right)(\partial_m U_j)\,\widehat{u}_m - \nu |\kappa|^2 \widehat{u}_k, \tag{7.27}$$

and

$$\partial_t \kappa_k = -(\partial_k U_m)\kappa_m. \tag{7.28}$$

Note that the velocity gradient tensor appears transposed in (7.28) with respect to (7.27). Note also that, because (7.28) is an evolution equation for the characteristic length scales of the fluctuations, initially isotropic fluctuations do not stay isotropic under deformation. The question of whether RDT remains valid indefinitely is more subtle, since formally (7.22) only applies if the fluctuations are infinitesimally small with respect to the base flow, so that no amount of amplification can make $\widetilde{u}$ comparable to U. In practice, however, the initial fluctuations have some non-zero amplitude and, if they are indefinitely amplified, their internal gradients $O(\kappa\widetilde{u})$ eventually become of the same order as $|\nabla \boldsymbol{U}|$. After that, the self-deformation times become of the same order as the rate of distortion by the base flow, and the linear assumption becomes invalid. Often this happens before viscosity has time to act, and the viscous term in the amplitude equation (7.27) can be neglected. What happens next can usually be approximated as a classical Kolmogorov cascade. Consider the following example.

Problem 7.3: Uniformly strained turbulence. Consider the case in which an initially turbulent flow is subject to axisymmetric axial stretching, so that that gradient matrix has the form

$$\nabla \boldsymbol{U} = \begin{pmatrix} 2\gamma & 0 & 0 \\ 0 & -\gamma & 0 \\ 0 & 0 & -\gamma \end{pmatrix}. \tag{7.29}$$

This may be a reasonable model for small-scale turbulence passing through an axisymmetric contraction, such as at the inlet of a wind tunnel. If the area of the nozzle is $A(x)$, the axial velocity is $U_c = F/A$, where F is the volumetric flux. The axial stretching would be $2\gamma \approx \mathrm{d}U_c/\,\mathrm{d}x_1 \approx -FA^{-2}(\,\mathrm{d}A/\,\mathrm{d}x_1)$. As the fluid element proceeds along the nozzle axis, the time it takes to reach a particular position is given by integrating

$$\frac{\mathrm{d}x_1}{\mathrm{d}t} = U_c, \qquad t = F^{-1}\int_{x_{10}}^{x_1} A\mathrm{d}x_1, \tag{7.30}$$

which can be inverted to obtain the time evolution of γ. If for example

$$A(x_1) = \frac{a}{x_1^2}, \quad \Rightarrow \quad \gamma = \frac{Fx_1}{a} = \frac{Fx_{10}/a}{1 + Fx_{10}t/a}. \tag{7.31}$$

Assuming that the total distortion,

$$G = \int_0^t \gamma \mathrm{d}t = \int_0^t \frac{\mathrm{d}U_c}{U_c} = \log\frac{A(0)}{A(t)}, \tag{7.32}$$

grows without bound with time, and neglecting viscosity, use the RDT equations to compute the asymptotic structure of the turbulence for large times, and estimate when, if ever, the linearized equations lose validity.

Note that, because of (7.32), the total distorsion is essentially the overall area ratio across the nozzle, and does not depend on the detailed area rule. In practice the detailed form of $A(x_1)$ is important, because it controls the behaviour of the boundary layers along the walls and the uniformity of the flow in each cross section.

Solution: The wavenumber evolution equation (7.28) takes the form

$$\begin{aligned} \partial_t \kappa_1 = -2\gamma\kappa_1, \qquad &\Rightarrow \qquad \kappa_1 = \kappa_{10}\exp(-2G) \\ \partial_t \kappa_j = \gamma\kappa_j, \qquad &\Rightarrow \qquad \kappa_j = \kappa_{j0}\exp(G), \quad j = 2,\, 3, \end{aligned} \tag{7.33}$$

showing that, as the fluctuations are stretched, the axial wavelengths become longer, while the radial ones are compressed. For large times we can assume that $\exp(G) \gg 1$, so that the wavenumber magnitude is

$$|\kappa|^2 \approx (\kappa_{20}^2 + \kappa_{30}^2)\exp(2G) = |\kappa_0|^2\exp(2G), \tag{7.34}$$

unless $\kappa_{20} = \kappa_{30} = 0$. The matrix in the right-hand side of the amplitude equation is, in that limit,

$$-\begin{pmatrix} 1 & 0 & 0 \\ 0 & 1-2\kappa_2^2/|\kappa|^2 & -2\kappa_2\kappa_3/|\kappa|^2 \\ 0 & -2\kappa_2\kappa_3/|\kappa|^2 & 1-2\kappa_3^2/|\kappa|^2 \end{pmatrix} \nabla \boldsymbol{U} \approx \gamma \begin{pmatrix} -2 & 0 & 0 \\ 0 & (\kappa_{30}^2-\kappa_{20}^2)/|\kappa_0|^2 & -2\kappa_{20}\kappa_{30}/|\kappa_0|^2 \\ 0 & -2\kappa_{20}\kappa_{30}/|\kappa_0|^2 & (\kappa_{20}^2-\kappa_{30}^2)/|\kappa_0|^2 \end{pmatrix}. \tag{7.35}$$

The streamwise perturbations decay as

$$\widehat{u}_1 \approx \widehat{u}_{10} \exp(-2G), \tag{7.36}$$

while the two transverse amplitudes have solutions which are proportional to $\exp(\pm G)$. Only the positive exponent is relevant for long times, and

$$\widehat{u}_2 \approx \frac{\kappa_{30}\widehat{u}_{20} - \kappa_{20}\widehat{u}_{30}}{\kappa_{30}^2 + \kappa_{20}^2} \kappa_{30} \exp(G), \tag{7.37}$$

$$\widehat{u}_3 \approx -\frac{\kappa_{30}\widehat{u}_{20} - \kappa_{20}\widehat{u}_{30}}{\kappa_{30}^2 + \kappa_{20}^2} \kappa_{20} \exp(G). \tag{7.38}$$

Note that $\widehat{u}_0$ and κ_0 are not exactly initial conditions in these equations, because we have used an approximation that is only valid for long times, but they are usually representative of the velocity magnitude and of the length scale of the fluctuations before they enter the contraction.

According to (7.37)–(7.38) the longitudinal fluctuations are quickly damped by the stretching, proportionally to the square of the area ratio, but the transverse ones are amplified. The latter is only apparent, because most of the amplification lies outside the range of validity of the linear approximation. As the transverse fluctuations grow, their transverse gradients increase as $\kappa\widehat{u} \sim \exp(2G)$, and become comparable to the rate of stretching when $\kappa_0\widehat{u}_0 \exp(2G) \approx \gamma$. This takes a time of order $\gamma^{-1}\log(\gamma/\kappa_o\widehat{u}_0)$, and at that moment

$$\widehat{u}_{max} \approx \widehat{u}_0 \exp(G) \approx \frac{\gamma A(t)}{\kappa_0 A(0)} \approx \frac{\gamma}{\kappa}, \tag{7.39}$$

which decreases as the total distortion increases. Beyond that moment the fluctuations become strong enough to decouple from the stretching, and decay through a standard turbulent, roughly isotropic, cascade. The characteristic decay time of this cascade is the eddy-turnover time of its largest-scale fluctuations, which is the inverse of $\kappa\widehat{u}_{max} \approx \gamma$. This is roughly the time that the fluid take to cross the contraction. Passing turbulence through a nozzle therefore damps it in a time scale γ^{-1}, instead of what would have been its unstrained decay time $(\kappa_0\widehat{u}_0)^{-1}$, by stretching directly the streamwise fluctuations, and by shrinking the transverse ones until their nonlinear cascade times also become of that order.

Supplementary questions: Using the results in appendix B, give reasonable expressions for the Fourier coefficients of the velocity components in a typical initially isotropic turbulent field.

Estimate the temporal evolution of the longitudinal and transverse spectra of the different velocity components,

$$E_{jj}(\kappa_k) \sim \frac{|\widehat{u}_j|^2}{\kappa_k}, \tag{7.40}$$

when subject to the rapid stretching (7.29), and the behaviour of the cutoff wavenumber for validity of the RDT approximation. Justify the expression (7.40) of the one-dimensional energy spectra.

Show that (7.27)–(7.28) imply that,

$$\partial_t(\kappa_k\widehat{u}_k) = 0, \tag{7.41}$$

so that, if the initial conditions are such that the flow is incompressible, it stays so forever. Note for example that the divergence of $\widetilde{u}$ in the previous solution grows as $\exp(2S)$, but that the form of (7.37)–(7.38) is such that the coefficient of the exponential vanishes.

The distortion of turbulence by other base flows can be treated in the same way as in the previous problem, and some examples are important in the evolution of shear flows. One of

them is the effect of a uniform shear, $\boldsymbol{U} = (Sx_2,\, 0,\, 0)$. The result in that case is that the two wavenumbers κ_1 and κ_3 are not modified, but that

$$\kappa_2 = \kappa_{20} - S\kappa_{10}t, \tag{7.42}$$

as the initial perturbations are tilted by the shear. Unless $\kappa_{10} = 0$ the result is that $|\kappa|$ increases linearly with t for large times, so that the viscous term can not be neglected and viscosity quickly damps the initial perturbations. The only fluctuations that survive are the infinitely long ones for which $\kappa_{10} = 0$, in which case all the components of κ remain constant, and the flow stays effectively inviscid if it was initially so. The amplitude equations for these modes are

$$\partial_t \widehat{u}_2 = \partial_t \widehat{u}_3 = 0, \tag{7.43}$$

$$\partial_t \widehat{u}_1 = -S\widehat{u}_2. \tag{7.44}$$

Equations (7.43) tell us that the cross-stream velocity component of these infinitely-long structures does not decay except by viscosity. This cross flow is incompressible and its evolution is decoupled from that of $\widehat{u}_1$. Equation (7.44) tells us that $\widehat{u}_1$ increases linearly with time, since $\widehat{u}_2$ is constant. In fact (7.44) is just the equation for the advection of the base shear S by the vertical velocity

$$\partial_t \widetilde{u}_1 + S\widetilde{u}_2 = 0, \tag{7.45}$$

What the RDT equations say in this limit is that infinitely long streamwise vortices are not modified by the shear, since there is no stretching along their axes. The vertical velocities induced by those vortices deform the velocity differences of the base flow into infinitely long 'streaks' of different streamwise velocity, taking fast particles into layers in which the mean velocity is slower, and viceversa. The process continues until the transverse gradients generated in this way are of the same order as S. This happens as soon as $\widetilde{u}_1 = O(SL)$, where L is the characteristic transverse dimension of the cross-flow eddies, which is determined by the initial conditions, and is not changed by the deformation. This can generate very strong perturbations of $\widetilde{u}_1$ that, since the linear growth in (7.45) is much slower than the exponential one found in problem 7.3, may last for long times. These streamwise streaks are a common feature of shear flows, and they almost inevitable form in any turbulent flow in the presence of shear.

Comment 7.4: Rather than the magnitudes $|\widehat{u}_j|^2$ of the Fourier coefficients of the different turbulent quantities, what are usually needed are their spectral densities, or the spectra that can be obtained from them by integration. Because the wavenumbers change with time in the RDT representation, and the Fourier coefficients are associated with the original wavenumbers at $t = 0$, care is needed to make sure that the evolution of the coefficients reflects that of the spectrum. Consider for example a small initial volume $|\Delta^3_\kappa|(0)$ in wavenumber space. The spectral density in its neighbourhood is

$$\frac{1}{|\Delta^3_\kappa|(0)} \int_{\Delta_\kappa} |\widehat{u}_j|^2 \mathrm{d}^3\kappa.$$

As the flow evolves, both $|\widehat{u}_j|$ and $|\Delta^3_\kappa|$ may change, and the evolution equation (7.27) for $\widehat{u}_j$ has to be supplemented by the evolution of $|\Delta^3_\kappa|$ given by (7.28). Happily the flow of wavenumbers induced by an *incompressible* RDT flow is itself incompressible, so that $|\Delta^3_\kappa|$ remains constant and only the evolution of the amplitudes has to be taken into account when computing the spectrum. The easiest way to prove that

is to see (7.28) as the description of the flow of a wavenumber 'gas' whose velocity is $c_k = \partial_t \kappa_k$. The divergence of that velocity is

$$\partial_k c_k = -(\partial_k U_m)\, \delta_{mk} = -\partial_k U_k = 0,$$

and the wavenumber flow is incompressible.

7.2.2 *The linear stability of parallel flows*

An important class of flows that cannot be treated in terms of a uniform velocity gradient, but that can still be analysed quite completely, are parallel shear flows in which the base velocity is directed along the x_1 axis, and depends only on the transverse direction x_2,

$$\boldsymbol{U} = [U(x_2),\, 0,\, 0]. \tag{7.46}$$

Slender flows like the free shear layer can be approximated in this way. The approximation used in that case is that the time taken for the fluctuations to grow or decay is short compared with the time needed by the base flow to change appreciably, or that the wavelengths of the fluctuations are short compared to the characteristic evolution length of the mean profile. Consider for example the quasi-parallel approximation of the shear layer leading to (7.8). We can expect the turbulent fluctuations within the layer to be at most of wavelength $O(\theta)$, while the analysis in problem 7.3 suggests that they grow or decay in times which are of the order of the inverse of the mean shear $T_s = O(\theta/\Delta U)$. During that time the fluctuations are advected by the mean flow over a distance $x_1 = O(U_c T_s) = O(\theta/\beta)$, and move to regions in which the mean profile has thickened by an amount $C_L \beta x = O(C_L \theta)$. Since the empirical value for C_L is small, that implies that the mean profile changes little during the characteristic evolution time of the fluctuations. Their behaviour can then be *approximately* analysed using a steady parallel velocity profile like the one found in problem 7.2,

$$U = \mathrm{erf}(x_2). \tag{7.47}$$

The hydrodynamic stability of parallel flows is a well-developed field. Several of the books mentioned in the introduction devote chapters to it, specially those by Monin & Yaglom (1975) and by Lesieur (1997). Classic textbooks on flow stability are those by Betchov & Criminale (1967) and by Drazin & Reid (1981), and an excellent modern textbook, although primarily devoted to wall-bounded flows, is Schmid & Henningson (2001). The review articles by Ho & Huerre (1984) and Huerre (2000) deal with instabilities in free shear flows, and are specially relevant to the discussion in this chapter. The reader interested in the details of the stability theory should consult those references. We only discuss here the minimum necessary to understand the dynamics of free shear flows.

When considering perturbations to flows such as (7.46) it is convenient to eliminate the pressure from the equations by expressing them in terms of vorticity,

$$(\partial_t + U\partial_1)\widetilde{\omega}_1 + U'\partial_1 \widetilde{u}_3 = \nu \nabla^2 \widetilde{\omega}_1, \tag{7.48}$$

$$(\partial_t + U\partial_1)\widetilde{\omega}_2 + U'\partial_3 \widetilde{u}_2 = \nu \nabla^2 \widetilde{\omega}_2, \tag{7.49}$$

$$(\partial_t + U\partial_1)\widetilde{\omega}_3 + U'\partial_3 \widetilde{u}_3 - U''\widetilde{u}_2 = \nu \nabla^2 \widetilde{\omega}_3, \tag{7.50}$$

where U' and U'' stand for $\mathrm{d}U/\,\mathrm{d}x_2$ and $\mathrm{d}^2U/\,\mathrm{d}x_2^2$. The dependence on $\widetilde{u}_3$ can be eliminated by cross-differentiating (7.48) and (7.50), to obtain an equation which depends only on $\widetilde{u}_2$,

$$(\partial_t + U\partial_1)\Phi - U''\partial_1\widetilde{u}_2 = \nu\nabla^2\Phi, \tag{7.51}$$

where $\Phi = \nabla^2\widetilde{u}_2$. Recalling the vector identity

$$\nabla^2\boldsymbol{u} = \nabla(\nabla\cdot\boldsymbol{u}) - \nabla\times\nabla\times\boldsymbol{u}, \tag{7.52}$$

which for an incompressible fluid becomes

$$\nabla^2\boldsymbol{u} = -\nabla\times\boldsymbol{\omega}, \tag{7.53}$$

the quantity Φ is seen to be the component of the curl of the vorticity along x_2. For example, in a two-dimensional flow in the $(x_1 - x_2)$ plane, where $\widetilde{\omega}_3$ is the only component of the perturbation vorticity, $\Phi = \partial_1\widetilde{\omega}_3$, and a perturbation with $\Phi = 0$ which decays at infinity is necessarily irrotational.

This equation and (7.49) form an autonomous system that allows us to compute the behaviour of $\widetilde{u}_2$ and $\widetilde{\omega}_2$, and which is the basis for the analysis of the linear stability of parallel flows. It has to be supplemented with boundary conditions which usually require that the velocity perturbation vanish at the walls or at infinity. Equation (7.51) is associated with the names of Orr and Sommerfeld, and (7.49) is named after Squire. For the purpose of understanding free shear flows we only have to worry about the inviscid limit, in which case (7.51) is called Rayleigh's equation.

The stability equations are linear, and can be solved by superposition of elementary solutions, which are harmonic along the directions in which the basic flow is homogeneous. Moreover, if the basic flow is steady, the temporal behaviour of each individual mode can be expanded in terms of exponentials. Thus in the case of (7.46) the perturbations can be expanded in terms of functions of the form

$$\widetilde{u} = \widehat{u}(\kappa_1,\,\kappa_3,\,x_2)\exp[\mathrm{i}(\kappa_1 x_1 + \kappa_3 x_3) + \sigma t]. \tag{7.54}$$

If we substitute (7.54) into (7.51) the Orr–Sommerfeld equation reduces to

$$(U-c)\widehat{\Phi} - U''\widehat{u}_2 = -\frac{\mathrm{i}\nu}{\kappa_1}\left(\frac{\mathrm{d}^2}{\mathrm{d}x_2^2} - \overline{\kappa}^2\right)\widehat{\Phi}, \tag{7.55}$$

where $\overline{\kappa}^2 = \kappa_1^2 + \kappa_3^2$,

$$\widehat{\Phi} = \left(\frac{\mathrm{d}^2}{\mathrm{d}x_2^2} - \overline{\kappa}^2\right)\widehat{u}_2, \tag{7.56}$$

and $\sigma = -\mathrm{i}\kappa_1 c$. Because (7.55) is a homogeneous equation with homogeneous boundary conditions, it only has non-vanishing solutions if a certain eigencondition,

$$\sigma = \sigma(\kappa_1,\,\kappa_3), \tag{7.57}$$

is satisfied. We will only concern ourselves here with the (simplest) temporal problem, in which the spatial wavenumbers κ_1 and κ_3 are real and the temporal eigenvalue, $\sigma = \sigma_r + \mathrm{i}\sigma_i$,

can be complex. Eigenfunctions whose eigenvalues σ have positive real parts (so that the phase velocity c has a positive imaginary part) grow exponentially in time, while those whose eigenvalues have negative real parts decay. Any initial condition can be expanded in terms of all the spatial wavenumbers and, after a while, only those with unstable eigenvalues grow, and the stable ones disappear. From the point of view of long-term behaviour, only the former have to be studied. (Orr!!!!)

Neutral modes, whose eigenvalues are purely imaginary or zero, or even those which only grow or decay slowly, are special cases. In general they do not evolve fast enough to compete with other unstable modes, and they are swamped by them. They can however grow algebraically under certain conditions of symmetry and, if no exponentially unstable mode exists, they become dominant. They are of some interest in wall turbulence, but usually not in free shear flows, which tend to be exponentially unstable. We saw an example of algebraic growth when we discussed in (7.44) the formation of velocity streaks in a rapidly-sheared flow.

The instabilities of steady parallel flows can be classified into two groups. The 'inertial' ones are essentially independent of viscosity, and are unstable as long as the Reynolds number is above a low threshold, $Re \approx 1 - 10$. Their eigenvalues are of the same order as the shear of the base flow, and they grow in times comparable to a single turnover time of the basic flow. They can be studied in terms of the inviscid Rayleigh's stability equation. The instabilities of the second group appear in flows which are stable to perturbations of the first type, and they depend on viscosity for their destabilization mechanism. These flows are typically stable for very low and for very high Reynolds numbers, and unstable only in some intermediate range. The growth rates of this second class of instabilities tend to be much slower than those of the inertial type, and they are therefore not important in turbulence. On the other hand, they control transition in some wall-bounded cases.

There are several features that simplify the study of the solutions of the stability equations (7.55)–(7.56). If we just consider the inviscid case, the wavenumber vector only enters the problem through its magnitude $\overline{\kappa}$, so that the eigenvelocities can only be functions of $\overline{\kappa}$. Since moreover the growth rate of the unstable fluctuations is the real part of σ,

$$\sigma_r = \kappa_1 c_i = (\overline{\kappa}^2 - \kappa_3^2)^{1/2} c_i(\overline{\kappa}) \leq \overline{\kappa}\, c_i(\overline{\kappa}), \tag{7.58}$$

the most unstable eigenmodes are those with $\kappa_3 = 0$. They correspond to two-dimensional waves which are uniform in the spanwise direction. The behaviour of oblique waves, in which $\kappa_3 \neq 0$, can be deduced directly from the transformation (7.58), and only the two-dimensional case has to be studied. Even in the viscous case oblique waves can be transformed into two-dimensional ones by changing the viscosity to

$$\nu' = \overline{\kappa}\, \nu / \kappa_1 \geq \nu. \tag{7.59}$$

Since in free shear flows a higher viscosity is generally stabilizing, it is usually sufficient to consider two-dimensional waves when looking for unstable solutions. Note however that Squires equation (7.49) is forced by the Orr–Sommerfeld solutions, rather than being a homogeneous problem. It contains κ_3 explicitly and becomes trivial in the two-dimensional limit. Two-dimensional fluctuations only contain spanwise vorticity, and the study of the other two vorticity components requires the consideration of oblique waves.

Another simplifying property of inviscid flows is that the equation (7.55) becomes real. Its eigenvelocities are therefore either real or form conjugate complex pairs. In the first case the fluctuations are neutral, moving as waves with an advection velocity c_r. In the case of conjugate pairs one of the velocities has a positive imaginary part, and the fluctuations are unstable with a growth rate $\kappa_1 c_i$. Only in the presence of viscosity can all the eigenvalues of the Orr–Sommerfeld equation be stable.

In the absence of rotation and body forces, the instabilities of Rayleigh's equation are always associated to the presence of layers of stronger vorticity in a weaker background (Rayleigh, 1880). This is the basic Kelvin–Helmholtz instability discussed in §2.2, in which the vorticity layer breaks down, essentially by wrinkling, in times which are of the order of its internal shear time. Because of their fast growth rates, which operate in inertial time scales, such instabilities are crucial in the development of free-shear flows.

Comment 7.5: To prove Rayleigh's criterion, write the inviscid version of equation (7.55) as

$$\frac{\mathrm{d}^2\widehat{u}_2}{\mathrm{d}x_2^2} - \left(\overline{\kappa}^2 + \frac{U''}{U-c}\right)\widehat{u}_2 = 0, \tag{7.60}$$

multiply it by the complex conjugate u_2^*, and integrate over x_2. Using the homogeneous boundary conditions to drop total differentials after integration by parts, the resulting equation is

$$\int U''(U-c^*)\frac{|\widehat{u}_2|^2}{|U-c|^2}\mathrm{d}x_2 = -\int \left(\overline{\kappa}^2|\widehat{u}_2|^2 + |\,\mathrm{d}\widehat{u}_2/\,\mathrm{d}y|^2\right)\mathrm{d}x_2 \leq 0. \tag{7.61}$$

The imaginary part of this equation is

$$c_i \int U''\frac{|\widehat{u}_2|^2}{|U-c|^2}\mathrm{d}x_2 = 0, \tag{7.62}$$

which shows that, either $c_i = 0$, which is the neutral case, or the integral vanishes. The latter can only happen if there is an inflection point in the velocity profile, where U'' changes sign and which correspond to either vorticity minima or maxima.

To prove that only vorticity maxima are unstable, consider the real part of (7.61),

$$\int U''(U-c_r)\frac{|\widehat{u}_2|^2}{|U-c|^2}\mathrm{d}x_2 < 0. \tag{7.63}$$

It follows from (7.62) that, if the fluctuations are not neutral, we can substitute c_r in (7.63) by any constant c_a, and that the combination $U''(U-c_a)$ has to be negative over a large enough interval for the integral in (7.63) to be negative. Choosing c_a to be the mean velocity of the base flow at the inflection point we obtain, for sufficiently monotonic profiles, a condition that has to be satisfied by the extremum of the vorticity at that point. It is easy seen by a little experimentation that the only possibility is a maximum of the vorticity magnitude.

Rayleigh's criterion is not sufficient. A counterexample was given by Tollmien (1935), who showed that the case $U = \sin(x_2)$ is stable. He however gave arguments suggesting that inflection points are probably always unstable in monotonic velocity profiles, and in practice most isolated vorticity layers are found to be unstable.

7.2.3 *The application to free shear layers*

If we approximate as before the shear layer by a uniform vorticity layer of non-zero thickness, we can choose frame of reference moving with the average of the two velocities, in which the two streams are counterflowing. The problem is then approximately antisymmetric across the layer, and the perturbations grow without moving to the right or to the

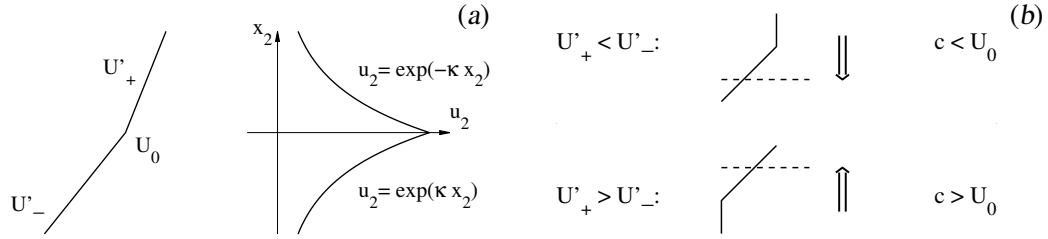

FIGURE 7.5. (*a*) Definition and eigenfunction for waves on a corner profile. (*a*) Displacement of the phase velocity for concave and convex corners.

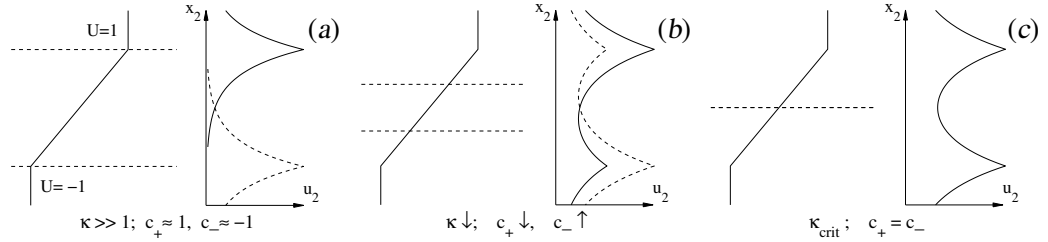

FIGURE 7.6. Evolution of the eigenfunctions and eigenvalues for the piecewise-linear approximation to the shear layer profile, as a function of wavenumber. At large wavenumbers two narrow eigenfunctions exist (*a*), associated with both corners, and with different phase velocities close to those of the two streams. As the wavenumber decreases (*b*) the phase velocities come closer to each other, as the eigenfunctions become wider begin to mix. For the critical wavenumber in (*c*) the eigenvalues merge, and so do the eigenfunctions. Beyond that, the layer becomes unstable.

left. This implies that, in the laboratory frame, the instability waves travel with a velocity which is the average of both streams. The mechanism described in §2.2 for the Kelvin-Helmholtz instability is robust, and works in spite of possible imperfections of the vorticity layers, which are therefore almost always unstable. It is also essentially independent of the Reynolds number, but the requirement that the layer should deform as a whole limits the instability to relatively long wavelengths. We will see below, as an example, that a shear layer with a hyperbolic tangent velocity profile is only unstable to perturbations whose wavelengths are longer than $12\,\theta$, and that the maximum growth rate occurs for wavelengths approximately equal to $30\,\theta$. A consequence of the inviscid nature of the instability is that it also works for turbulent flows such as the one in figure 7.4(*a*). The large structures feel the effect of the smaller ones as an eddy viscosity, which is different from the molecular viscosity, but which only has a minor effect on their behaviour.

Many of the complications of Rayleigh's equation can be avoided by studying profiles such as the one in figure 7.5(*a*), which are formed by straight line segments. On each of these segments, $U'' = 0$, and the equation reduces to $\widehat{u}_2'' - \overline{\kappa}^2 \widehat{u}_2 = 0$, whose solutions are $\widehat{u}_2 \sim \exp(\pm\overline{\kappa} y)$. At the corners the second derivative is infinite, but the equation can be integrated across the singularity to obtain a jump condition which contains all the required information,

$$(U_0 - c)\,[\,\mathrm{d}\widehat{u}_2/\,\mathrm{d}x_2]_-^+ = \widehat{u}_2\,[U']_-^+. \tag{7.64}$$

For the single corner in figure 7.5(*a*), this condition, together with the form of the eigen-

functions above and below the corner, results in

$$c = U_0 + \frac{U'_+ - U'_-}{2\overline{\kappa}}. \tag{7.65}$$

The shift in the wave propagation velocity with respect to the velocity at the corner is shown in figure 7.5(*b*). For convex corners, the propagation velocity moves down, towards lower velocities. For concave ones it moves up.

There is a simple interpretation for this shift. Because of the exponential decay of the eigenfunctions, the perturbation is centred at the corner, with a decay length $\sim 1/\overline{\kappa}$. It is concentrated in a narrow layer for high wavenumbers, and spreads out for lower ones. The propagation velocity is some average of the fluid velocity over the layer on which the wave exists. Equation (7.65) can be written as

$$c = \frac{1}{2}\left[U(1/\overline{\kappa}) + U(-1/\overline{\kappa})\right]. \tag{7.66}$$

The layer in which the magnitude of the velocity gradient is strongest wins, and the propagation velocity shifts towards it, as shown in the figure.

Most of the velocity perturbation in these corner waves is irrotational, because $\widehat{\Phi} = 0$. This is because the vorticity on each side of the corner is constant, and the two-dimensional velocity perturbations cannot create vorticity inhomogeneities by advecting it. The vorticity perturbations reside in this case in the corner of the velocity profile, where the velocity gradient is discontinuous. The perturbations in $\widetilde{u}^2$ deform the interface between the two streams and create what appears as a vorticity wave propagating along the corner. The circulation density in this wave can be computed by applying continuity at both sides of the corner

$$[\widehat{u}_1]^+_- = \frac{\mathrm{i}}{\kappa_1}[\,\mathrm{d}\widehat{u}_2/\,\mathrm{d}x_2]^+_- = \mathrm{i}\,\frac{[U']^+_-}{\kappa_1(U_0 - c)}\widehat{u}_2. \tag{7.67}$$

In smoother profiles the vorticity wave spreads over a thicker layer, but it is always associated with the second derivative of the mean velocity.

We are now in position to understand the instability of a velocity profile with a single inflection point, and to get a better feeling for the reasons for Rayleigh's criterion. Since we have seen that the eigenvalues of Rayleigh's equation can only be real, in which case the stability is neutral, or complex conjugate pairs, which is the unstable case, and since the eigenvalues are continuous functions of the parameters of the problem, the transition from one to the other can only occur if two eigenvalues merge into a double one on the real axis, from where they separate again either as a neutral real or as an complex unstable one[1].

Consider very short shear waves on a piecewise-linear velocity profile like the one in figure 7.6(a), which is an approximation to a vorticity layer. It is clear from the previous discussion that waves can be sustained either in the upper or in the lower corner of the profile, with eigenfunctions concentrated in the neighbourhood of each corner, and with phase velocities approximately equal to the fluid velocity in the upper and lower streams, $U = \pm 1$. As we lower the wavenumber to consider longer waves (figure 7.6*b*), the eigenfunctions widen,span a larger fraction of the profile, and, as seen above, their phase velocities come

[1]This process is sometimes referred to as a 1:1 resonance.

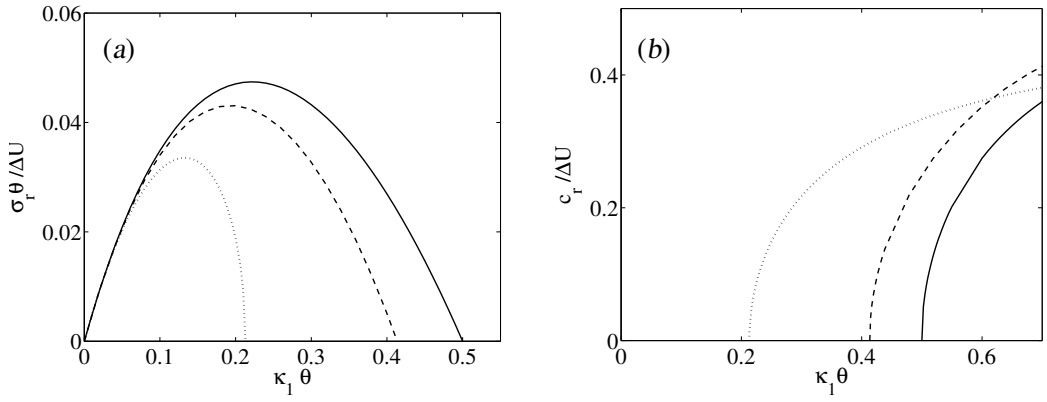

FIGURE 7.7. Eigenvalues of different models for the shear layer velocity profile. ——— , $U = \tanh(x_2)$; - - - - , $U = \mathrm{erf}(x_2)$; ····· , straight-line approximation. (*a*) Growth rate $\kappa_1 c_i$ of the unstable waves. (*b*) Real phase velocity of the upper stable waves. As $\kappa_1\theta \gg 1$, the phase velocities of the three cases tend to the free-stream value $c_r = \Delta U/2$.

closer to each other. At the same time the eigenfunctions themselves, although still preferentially associated to the upper or to the lower corner, extend into each other and become more symmetric. Eventually (figure 7.6*c*) they merge, and so do their phase velocities. It is only after that collision of the eigenvalues that the two velocity split into into a complex conjugate pair, one of whose components is unstable.

Problem 7.6: Use piecewise-exponential eigenfunctions, and the jump condition (7.64) to compute the eigenvalues of the straight-line profile

$$U = \begin{cases} 1, & x_2 > 1 \\ x_2, & -1 \le x_2 \le 1 \\ -1, & x_2 < -1 \end{cases} ,$$

and compare them with the results in figure 7.7

Answer:

$$c = \frac{\left[(2\kappa_1 - 1)^2 - \mathrm{e}^{-4\kappa_1}\right]^{1/2}}{2\kappa_1}$$

More realistic models for a vortex layer than the piecewise-linear one just discussed are the smooth error-function profile found in problem 7.2, or the rather similar

$$U(x_2) = \frac{1}{2}\tanh(x_2) \tag{7.68}$$

which was studied first by Michalke (1964), and which has been used since then as the standard approximation for the stability properties of free shear layers. Their eigenvalues are represented in figure 7.7. The general behaviour is similar in the three cases, especially for the longer waves, but the shorter ones near the stability threshold are sensitive to the difference between the sharp corners of the piecewise approximation and the smoother ones of the other two profiles.

The character of the eigenfunctions is the same as those sketched in figure 7.6. The neutral high-wavenumber waves are concentrated near one or the other edge of the layer, and

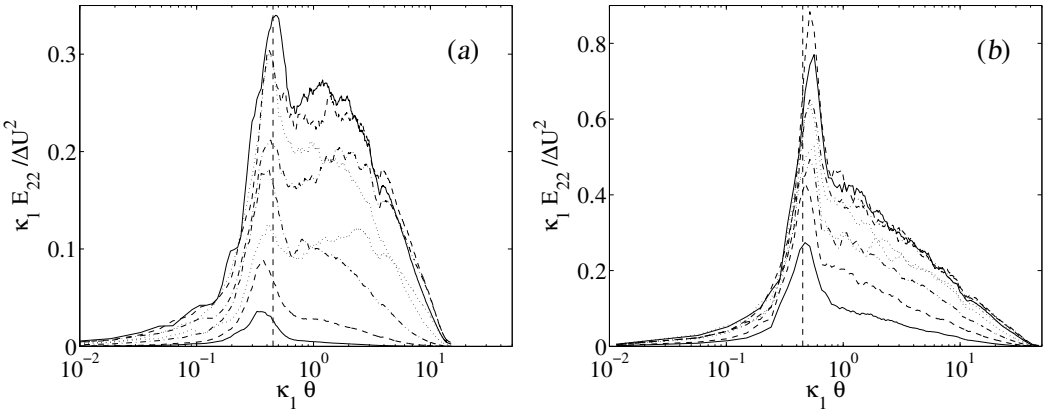

FIGURE 7.8. (*a*) Energy spectra of the transverse velocity component in a free shear layer, plotted against the wavenumber normalized with the local momentum thickness, from Delville, Bellin & Bonnet (1988). The dashed vertical line is the limit of instability for a parallel error function velocity profile, $\kappa_1\theta = 0.42$. The different spectra correspond to different positions across the layer. $\beta = 0.3$. $\Delta U\theta_0/\nu = 2.2 \times 10^3$. (*a*) $\Delta U\theta/\nu = 3.9 \times 10^3$, $\beta x/\theta_0 = 35$. (*b*) $\Delta U\theta/\nu = 1.2 \times 10^4$, $\beta x/\theta_0 = 140$.

their phase velocities tend to those of the free streams as κ_1 increases. There is one family of neutral waves associated to each edge of the layer, whose velocities are respectively positive and negative for symmetric profiles such as (7.68). In a shear layer between streams with velocities U_a and U_b, such as the one discussed in §7.1, the mean velocity $U_c = (U_b + U_a)/2$ should be added to all the eigenvalues, and the two families of neutral waves move respectively faster and slower than U_c.

The eigenfunctions become more symmetric for longer wavelengths, until both families merge at the stability limit. Beyond that limit the eigenfunctions become complex conjugates, with a $\widehat{u}_2$ eigenfunction which is symmetric in x_2. This means that the transverse velocities of the unstable waves oscillate in phase in the two streams, and that the layer meanders as a whole, rather than being deformed internally. The real part of the phase velocity for the unstable waves is always U_c, suggesting that this should be the velocity of the large scale structures observed in experimental layers. This prediction is found to be very approximately correct.

The structure of experimental shear layers can be related fairly closely to the predictions of the stability analysis. Figure 7.8 shows spectra of the transverse velocity, which correspond to the squared amplitude of $\widehat{u}_2$ eigenfunctions discussed above. The Reynolds number in figure 7.8(*b*) is comparable to that in the right-hand end of the upper shear layer in figure 7.4, while that in figure 7.8(*a*) is closer to the 10% station of the same layer. In both cases the figure contains spectra at several cross-stream locations, and the fact that the energy peaks agree across the layer supports the model that they are dominated in each case by a single coherent wave spanning the flow. The dashed vertical line is in both cases the stability limit $\kappa_1\theta \approx 0.45$ found in figure 7.7 for the two continuous approximations to the mean velocity profile. It is clear that the spectra are divided into distinct regions by that threshold. To the left, in the unstable region, there is a roughly exponential growth with wavenumber, while to the right there is a milder decay.

This behaviour was first explained by Ho & Huerre (1984) who noted that, since the momentum thickness θ is proportional to x_1, a wave with a fixed wavenumber κ_1 moves to the right in the $\kappa_1\theta$ stability diagram as it travels downstream. As long as $\kappa_1\theta$ is below the stability threshold the wave grows exponentially but, as it is carried beyond the threshold by the growth of the momentum thickness, it stops growing and the regular turbulent dissipation processes begin to damp it algebraically. Note that this means that the dominant waves at each stations are not those whose wavelengths are amplified faster, but those which have been growing for a longer time. To the left of the stability threshold the structures are essentially linear, but to its right the linear RDT processes are not fast enough, and nonlinearity controls the flow. This is where turbulence resides.

An interesting observation is that, in this approximation, each wave is only amplified by the linear instability by a finite amount, and that the total amplification factor is independent of the wavenumber. Consider a profile for which the imaginary part of the eigenvelocity is

$$c_i = \Delta U f(\widehat{\kappa}), \quad \text{where} \quad \widehat{\kappa} = \kappa_1\theta, \tag{7.69}$$

and assume that $\theta = C_L\beta x_1$. Since the real phase velocity of unstable waves is constant, their wavelengths do not change as they are advected downstream. The evolution of their amplitudes is given by

$$\frac{1}{\widehat{v}}\frac{\mathrm{d}\widehat{v}}{\mathrm{d}t} = \frac{U_c}{\widehat{v}}\frac{\mathrm{d}\widehat{v}}{\mathrm{d}x_1} = \kappa_1\Delta U f(\widehat{\kappa}), \tag{7.70}$$

where $\widehat{v}$ stands for the amplitude of any of the velocity components. Equation (7.70) can be cast in such a way that $\widehat{\kappa}$ becomes the evolution variable, which varies between $\widehat{\kappa} = 0$ at $x = 0$ and the stability threshold $\widehat{\kappa}_s$ at which the wave stops growing. The result is

$$\frac{C_L}{2}\frac{1}{\widehat{v}}\frac{\mathrm{d}\widehat{v}}{\mathrm{d}\widehat{\kappa}} = f(\widehat{\kappa}), \qquad \widehat{v}(\widehat{\kappa}) = \widehat{v}(0)\,\exp\left(2C_L^{-1}\int_0^{\widehat{\kappa}} f(\xi)\mathrm{d}\xi\right). \tag{7.71}$$

For any of the two smooth profiles whose eigenvalues are given in figure 7.7, using the experimental value $C_L \approx 0.04$, the maximum amplification factor is

$$\widehat{v}(\widehat{\kappa}_s)/\widehat{v}(0) \approx 8 - 10. \tag{7.72}$$

Equation (7.71) suggests that, when expressed in terms of $\widehat{\kappa}$ as in figure 7.8, the velocity spectra to the left of the stability threshold should be similar at all streamwise stations of the layer. This is approximately satisfied by the spectra in the figure, but the details, and in particular the absolute amplitude, depend on the intensity $\widehat{v}(0)$ with which each wavenumber is forced at the exit from the splitter plate.

The amplification behaviour of the large structures in shear layers can be studied best by applying to them intentional small perturbations. A particularly careful study of this kind was done by Gaster, Kit & Wygnanski (1985), who studied the spatially-growing non-parallel stability problem, and found amplification factors lower than those in (7.72), of the order of 10–20. They also found that not only the growth rates, but even the structure of the large flow scales, agree well with those predicted by linear theory up to the neutral limit.

In a related experiment Oster & Wygnanski (1982) forced a turbulent shear layer near the splitter plate at frequencies that were far from the most amplified waves at that location,

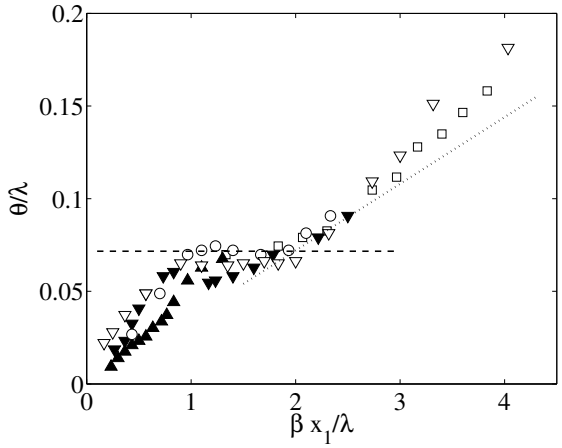

FIGURE 7.9. Growth of the momentum thickness of shear layers forced at the exit of the splitter plate with perturbations of frequency λ/U_c. Adapted from Browand & Ho (1987). Various experimenters and velocity ratios. The dashed horizontal line is equation (7.73). The dotted line is the unforced growth rate in figure 7.3(*b*).

but which became unstable farther downstream. Structures with the right wavelengths appeared as soon as the profile had grown enough for the forcing to be amplified. The growth of the thickness of the shear layers in several of these forced experiments is summarized in figure 7.9. The initial growth of the shear layer depends of the forcing frequencies and amplitudes but, as soon as the thickness becomes large enough for those initial waves to stop being amplified, the growth ceases until other 'natural' initial perturbations become strong enough to resume normal growth. We can relate the thickness plateau to the wavelength λ of the initial forcing using the linear stability limit

$$\kappa_1\theta = \frac{2\pi\theta}{\lambda} \approx 0.45, \quad \Rightarrow \quad \frac{\theta}{\lambda} \approx 0.07, \tag{7.73}$$

which is the dashed horizontal line in figure 7.9. The fact that the layer resumes essentially normal growth after the relatively-strong excursion away from it created by the initially-fast growth and later stagnation of the forced wavelength, strongly supports that the different wavelengths behave independently, and the process is linear.

The dependence of the shear-layer behaviour on the initial conditions implies that it can be intentionally controlled by relatively small perturbations introduced at the layer origin, and also that experimental observations can be modified by unintended environmental perturbations. This is thought to be one of the reasons for the relatively large scatter in the available experimental parameters for this flow, which can for example be seen in the growth rates given in figure 7.3(*b*).

7.2.4 *The nonlinear evolution*

After the vorticity waves stop being linearly amplified, nonlinearity takes over. The final result of the Kelvin–Helmholtz instability is that the vorticity tends to concentrate and, in the nonlinear regime, collapses into discrete vortex blobs. The resulting vorticity distribution

can be approximately analysed as an infinite row of point vortices (actually spanwise vortex lines), which are subject to a new instability. The vortices wander away from the uniform row and orbit in pairs, in what can be seen as a discrete version of the instability of the vorticity layer.

In the point-vortex approximation this 'pairing' instability repeats itself at a larger scale, resulting into complex vortex clouds which are fairly coherent. If the smearing of the initial vorticity is taken into account, the result of the initial Kelvin–Helmholtz instability is not a row of point vortices, but a series of vorticity blobs. They behave at first like points but, as they begin to pair, they merge into larger cores by the process of mutual deformation and tearing which was described in chapter 2. The result is a new row of vorticity clouds, each of which has twice the circulation of the original ones. As the merging repeats itself, the behaviour of the newly created cores is again similar to that of point vortices, but leads to a discrete inverse cascade of growing vortex cores, instead of to loose vortex clouds. At each step, the circulation around each core doubles and so does the average separation between them. On dimensional grounds, the time between mergings also doubles, and the result is a system that grows linearly in the average, as in (7.1), but whose growth happens in discrete steps instead of smoothly. This discreteness needs not be obvious in the overall statistics, because random variations in the initial or in the boundary conditions of the flow are amplified exponentially by the instability, and each pairing happens at a slightly different location, smoothing the mean growth. One ongoing merging is seen in the low Reynolds number flow in figure 7.4(*b*), while the increase in the wavelength of the structures is clear in the turbulent case in figure 7.4(*a*).

This pairing picture is slightly different from the interpretation of the structures as linear instability waves of the local mean velocity profile. Since the pairing argument depends on the instability of the row of point vortices, the two interpretations are not incompatible, but they differ in detail, and both points of view help to explain different aspects of the behaviour of shear layers.

In the profile instability model, for example, it is possible for the structures to reform with the right wavelength even after the waves are artificially destroyed or prevented from forming. Such an experiment was done by Cimbala, Nagib & Roshko (1988) who studied the wake behind a porous screen. Wakes and jets behave similarly to shear layers, and contain structures which can also be explained as originating from the amalgamation of initial transitional instabilities. The screen in Cimbala's experiment, however, was too porous to shed vortices, and the corresponding wake was featureless, although fully turbulent, for several diameters downstream. After a while the linear instability of the profile asserted itself, and large distinct structures were observed.

Since the growth rate of the initial perturbations is proportional to $\Delta U/\theta_0$, and since those initial waves move with a phase speed U_c, we may expect the first pairing to happen at some multiple of $U_c\theta_0/\Delta U = \theta/\beta$. Empirically the first three pairings in flows originating from laminar boundary layers happen around $\beta x/\theta_0 \approx 100,\ 200,\ 400$ (Jiménez 1983). When the initial boundary layers are either turbulent, such as the one in figure 7.8, or subject to strong perturbations, the initial ordered two-dimensional wavetrain may never form, or forms only intermittently, and the layer transitions directly to turbulence. Even if the initial rollup happens, the pairing process may never become organized under those conditions, and the continuous drift in the position of the dominant wavelength is better explained by

the local instability process discussed above.

In the case of initially-laminar boundary layers, in which discrete pairing has been well documented, the first and second vortex mergings randomize the structures so much that the layer essentially forgets its initial conditions. Ho *et al.* (1991) measured the standard deviation of the period between the passing of successive vortices in several natural and forced shear layers with laminar initial conditions. They found a transition from an ordered to a disordered vortex street in the region $\beta x/\theta_0 = 100 - 150$, which corresponds roughly to the first pairing, and which is also where the layer begins to be self-similar (figure 7.3*a*). They showed that pairing is the key randomizing event by an interesting forcing experiment. When they forced the layer at its natural most-unstable frequency, the transition in the vortex-passing periods happened at the same location as in the unforced case. When they forced it at a twice-lower frequency, thus locking the first pairing, the transition was delayed to the location of the second one. They finally proved that the randomization is not due to the appearance of three-dimensional turbulence by reproducing the same behaviour in two-dimensional numerical simulations.

Pairing is the first event in the development of the shear layer in which nonlinearity is important, and the randomization reflects the sensitivity to initial conditions which is typical of nonlinear chaotic systems (see chapter 2).

The two descriptions based on instability waves and on discrete nonlinear pairing can be reconciled, at least qualitatively. There is no doubt that everything before the first pairing is basically the linear growth of the instability waves. The thickness of the layer grows little until those waves are strong enough to generate Reynolds stresses, and the first waves that appear are those which are amplified fastest for the initial momentum thickness. Their wavelength is $\lambda_0 \approx 30\,\theta_0$ (or $\kappa_1\theta_0 \approx 0.2$, see figure 7.7), and they keep growing while $2\pi\theta/\lambda_0 \leq 0.45$, which is when the layer is thin enough for them to be unstable. The first pairing happens when the waves stop growing and nonlinearity has time to act (Goldstein & Lieb 1988). From the two estimates above, that happens when $\theta/\theta_0 \approx 0.45/0.2$, or $\beta x_1/\theta_0 \approx 60$. This is not too far from the empirical values for initially-laminar layers given above, specially since the virtual origin in those cases is typically downstream of the real one.

The different forcing experiments mentioned in this section show on the other hand that this argument is not enough. The growth of the layer depends on the intensity of the instability waves, which can be changed by forcing. The nonlinear pairing also depends on having subharmonic perturbations that are not so strong as to become dominant without the need of nonlinear interactions, as was the case in the experiment by Ho *et al.* (1991), or which are so weak that they cannot take over even when the fundamental mode stops growing, as in the case of figure 7.9. Nevertheless, under a wide range of conditions, the argument in the previous paragraph approximately explains the experimental observations.

All the discussion up to this point has been strictly two-dimensional. It is clear from figure 7.4(*a*) that there are essentially two-dimensional structures in the mixing layer, since they are visible in that spanwise-averaged view of the flow. It is also clear from that picture that there are three-dimensional structures superimposed to the large-scale waves. The initial stages of the sequence of bifurcations to three-dimensionality have been studied in some detail, and the end result is a classical turbulent cascade in which the energy spectrum changes from the very steep slope characteristic of two-dimensional flows, to the $-5/3$ ex-

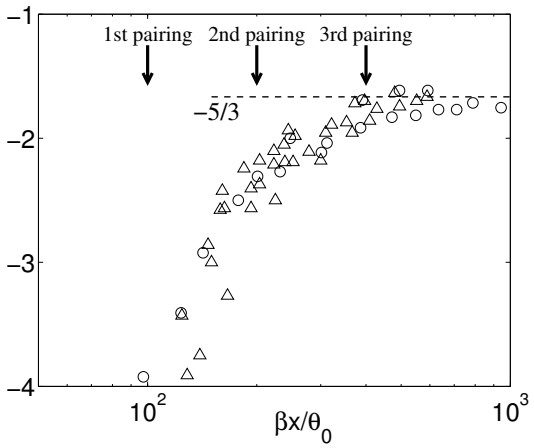

FIGURE 7.10. Downstream evolution of the logarithmic slope of the energy spectrum in a shear layer. The transition to fully three-dimensional turbulence is complete when the slope reaches the Kolmogorov value of $-5/3$. ○ , Jiménez (1983); △ , Huang & Ho (1990).

ponent of well-developed three-dimensional Kolmogorov turbulence (see figure 7.10). The speed of this transition is influenced both by the conditions of the initial boundary layers and by the pairing process but, as long as the initial Reynolds number is high enough, the transition to three-dimensional flow is complete at about the location which would correspond to the third pairing in an initially-laminar case.

7.2.5 *Mixing*

An important effect of the coherent structures is their influence on turbulent mixing which, as we noted at the beginning of this section, is one of the important applications of this particular kind of flows. Before the discovery of the structures it was known that the mean concentration profile of two mixing streams was similar to that of the velocity, and it was assumed that this reflected the molecular mixing of the two species. This turns out not to be the case in the presence of well-defined coherent structures, which move large parcels of unmixed fluid across the layer without actually mixing them, decreasing the rate of chemical reactions between the two streams. See for example in figure 7.4(*a*) how large tongues of almost pure fluid *A* cross into stream *B*, and viceversa. True mixing only occurs once these large-scale excursions have been broken to molecular size by the cascade process. Given a sufficiently high Reynolds number to allow for the development of a cascade, a 'mixing transition' occurs at $\beta x/\theta_0 \approx 200$, approximately coinciding with the location of the second pairing (Konrad 1976, Karasso & Mungal 1996), across which the amount of product generated in a chemical reaction between the two streams increases sharply.

As with any property depending of the generation of small scales, the location of the mixing transition depends on the level of perturbations in the initial conditions of the layer, and it can be moved closer to the origin by for example tripping the initial boundary layers to increase its three-dimensionality. This has been used to shorten the length of mixers and burners by shaping the trailing edge of the injecting nozzle in such a way that it introduces streamwise vorticity in the mixing layer.

	δ	u_1	Re	Remarks
Plane shear layer	x_1	ΔU	x_1	
Plane jet	x_1	$(D_1/\rho)^{1/2}x_1^{-1/2}$	$x_1^{1/2}$	
Round jet	x_1	$(D/\rho)^{1/2}x_1^{-1}$	constant	
Plane wake	$L(x_1/L)^{1/2}$	$U_\infty(x_1/L)^{-1/2}$	constant	$L = D_1/\rho U_\infty^2$
Round wake	$L(x_1/L)^{1/3}$	$U_\infty(x_1/L)^{-2/3}$	$x_1^{-1/3}$	$L = (D/\rho U_\infty^2)^{1/2}$

TABLE 7.1. Scaling laws for selected free-shear flows. u_1 represents the magnitude of the deviations of the mean velocity profile with respect to the flow velocity U_∞ of the free stream, as well as the scale of the turbulent velocity fluctuations. δ is the transverse dimension of the flow, and also the integral scale of the turbulence. The evolution of the Reynolds number $Re = u_1\delta/\nu$ determines whether the flow laminarizes or remains turbulent downstream. D_1 is the drag or the momentum flux per unit span in plane flows, and D is the total drag in axisymmetric ones.

7.3 Other free-shear flows

Because it is difficult to create a non-trivial velocity profile away from walls without at least one inflection point (**Problem:** *Try it*), the common characteristic of free shear flows is that they are subject to global inviscid instabilities. This gives them a set of common properties which they share with the plane mixing layer, such as being thin and slowly-spreading, and having large-scale structures of the order of the width of the flow and perturbation velocities of the order of the velocity difference across the shear. The presence of these large scales imply that these flows can be modelled by simple eddy viscosity approximations in which the eddy viscosity is constant across the flow thickness. It also that the magnitude of their eddy viscosities is not universal, because the large scales depend on the details of the imposed shear.

It is relatively easy to analyse the mean properties of many free shear flows by simple energy arguments such as the one used at the beginning of this chapter for the plane shear layer. Examples of how this is done for free jets and wakes are given in the next two problems, and a summary of the scaling properties of those flows can be found in table 7.1. Two apparently different derivations of the same results can be found in Schlichting (1968) and in Pope (2000). All of them are equivalent, and they all amount to dimensional arguments together with the assumption, which is valid because of the presence of large-scale instabilities, that the scaling of the turbulent structures follows the scaling of the mean flow.

Problem 7.7: The plane turbulent jet. A plane turbulent jet is formed when a stream is injected into a quiescent infinite fluid from a nozzle formed by two infinitely-wide parallel plates. A plane shear layer forms initially behind each plate, but they eventually grow enough to merge together, and the resulting turbulent jet only retains from its initial conditions the total momentum D_1 injected per unit span.

Determine the asymptotic evolution laws for the width δ of the jet and for its centreline velocity u_c, as a function of the downstream coordinate x_1. Compute the ingestion velocity with which the jet entrains fluid from infinity. Define a local Reynolds number $Re_\theta = u_1\theta/\nu$. How does it change with x_1? Use this evolution to predict whether the jet would become more or less turbulent as it moves away from the nozzle.

Solution: Consider the jet defined in figure 7.11, and write the conservation of horizontal momentum in a domain such the dashed rectangle in the figure, and of unit span. Since we expect the jet to grow only

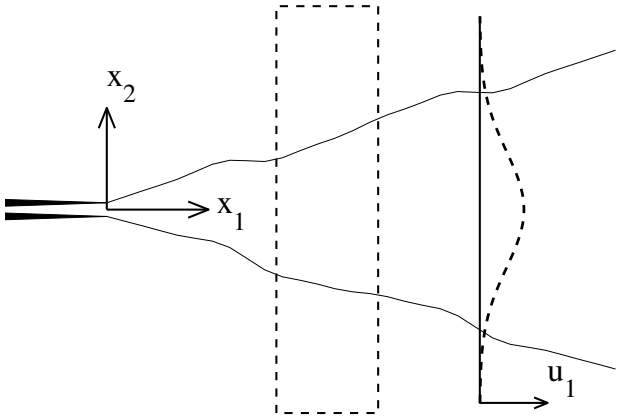

FIGURE 7.11. A plane turbulent jet

slowly downstream, we can use the boundary layer approximation developed in problem 7.2 to neglect the cross-stream variation of the pressure and, since the flow is quiescent at $x_2 \to \pm\infty$, to neglect any contribution of the pressure to the momentum equation. Also, because u_1 vanishes far from the jet, there is no horizontal momentum flux at the top and bottom limits of the control volume, and we deduce that the momentum flux per unit span through each vertical section

$$D_1 = \int_{-\infty}^{\infty} \rho u_1^2 \mathrm{d}x_2 \approx \rho u_c^2 \delta \tag{7.74}$$

is independent of x_1. We repeat next the energy dissipation argument used at the beginning of this chapter to estimate the growth rate of the plane shear layer. We obtain

$$\frac{\mathrm{d}\Phi}{\mathrm{d}x_1} \approx \rho \frac{\mathrm{d}(u_c^3 \delta)}{\mathrm{d}x_1} \approx -\rho\varepsilon\delta \approx -0.1\rho\delta\frac{u_c^3}{\delta}. \tag{7.75}$$

The last part of this equation assumes that the typical velocity of the large-scale eddies is of the same order of magnitude as the mean centreline velocity, and that the integral scale is of order δ. Combining (7.74) and (7.75), we obtain

$$\delta \approx 0.2x_1, \tag{7.76}$$

and

$$u_c \approx 0.5(D_1/\rho)^{1/2} x_1^{-1/2}. \tag{7.77}$$

The coefficient in (7.76) agrees well with the growth of the thickness of experimental jets, when δ is defined as the distance between the two points in which the mean velocity is $u_c/2$. Using an eddy viscosity approximation similar to the one in the plane shear layer, it can be shown that

$$u_1/u_c \approx \exp(-4\log 2[x_2/\delta]^2), \tag{7.78}$$

which agrees well with experiments. The numerical factor in the exponent is implied by the definition of δ. It follows from (7.78) that the volume flux in the jet increases as

$$\Phi_v = \int_{-\infty}^{\infty} u_1 \mathrm{d}x_2 = \sqrt{\pi}\, u_c \delta \approx 0.18(\rho x_1/D_1)^{1/2}, \tag{7.79}$$

which implies that fluid should be entrained from infinity as

$$u_{2,\infty} = -\frac{1}{2}\frac{\mathrm{d}\Phi_v}{\mathrm{d}x_1} = -0.044(\rho/D_1 x_1)^{1/2}. \tag{7.80}$$

This ingestion of outside fluid, which is important in the dilution of effluents from jets and in other mixing processes, is what prevent us from using the initial mass injection rate as an invariant to characterize the flow, instead of the momentum flux. Note that the local turbulent Reynolds number of the jet is proportional to Φ_v/ν and increases with increasing x_1. Therefore, if the initial Reynolds number is high enough to sustain turbulence, the flow would become ever more turbulent as it evolves downstream.

Problem 7.8: The axisymmetric wake. Repeat problem 7.7 for the axisymmetric wake behind a body whose drag is D.

Solution: The analysis used for the plane jet can be repeated here using slightly more complicated expressions for the fluxes of momentum and energy, which have to take into account the contribution of the free stream velocity, but it is easier to work in a frame of reference in which the fluid far from the wake is at rest. The body then moves with a velocity U_∞ and, in an equilibrium situation, the mean flow is a function of $\xi = x_1 - U_\infty t$. Therefore,

$$\partial_t = -U_\infty \partial_1. \tag{7.81}$$

If u_1 is the fluid velocity in this frame of reference, which would be the velocity defect with respect to infinity in a frame of reference moving with the body, the momentum equation integrated in a cross plane is

$$\partial_t \int u_1 \, \mathrm{d}S + \partial_1 \int u_1^2 \, \mathrm{d}S = \partial_1 \int u_1 (u_1 - U_\infty) \, \mathrm{d}S = 0. \tag{7.82}$$

As in the jet, the total momentum flux is independent of x_1, and can be made equal to the drag,

$$\int u_1 (U_\infty - u_1) \, \mathrm{d}S = D/\rho. \tag{7.83}$$

Similarly for the decay of the energy flux

$$\partial_1 \int u_1^2 (U_\infty - u_1) \, \mathrm{d}S \approx -\frac{u_1^3}{\delta} \delta^2. \tag{7.84}$$

Because of the presence of U_∞ in these equations, which acts as an explicit velocity scale, wakes are only self-similar in the limit in which $u_1 \ll U_\infty$, where we can approximate (7.83) by

$$U_\infty u_1 \delta^2 \approx D/\rho, \tag{7.85}$$

with a similar expression for (7.84). Finally we get

$$u_1/U_\infty \approx (x_1/L)^{-2/3}, \tag{7.86}$$

and

$$\delta/L \approx (x_1/L)^{1/3}. \tag{7.87}$$

$L = (D/\rho U_\infty^2)^{1/2}$ is a length scale of the order of $(c_D S)^{1/2}$, where c_D is the drag coefficients and S the frontal cross section of the body. The turbulent Reynolds number

$$\frac{u_1 \delta}{\nu} \approx \frac{U_\infty L}{\nu} (x_1/L)^{-1/3}, \tag{7.88}$$

decays downstream, and the wake relaminarizes eventually. This, together with the requirement that $x_1/L \gg 1$ before u_1/U_∞ is small enough for the flow to be considered self-similar, makes the axisymmetric wake a flow which is experimentally much less universal than others in this class.

Note that the previous analyses are only approximate, because they for example neglect the kinetic energy of the turbulent fluctuations in estimating the energy balance. This is not always very accurate, particularly in weakly-turbulent flows such as wakes, but it only adds numerical factors if the flow is self-similar.

7.3.1 *Control*

We have seen in the case of plane mixing layers several ways in which the growth rate of the layer, or its mixing properties, could be changed by acting on the level of perturbation in its initial conditions. This is a general property of flows with a clear instability mode, which is the defining characteristic of most free shear flows. It is clear that, if the large structures determine the energy dissipation rate and the Reynolds stresses, and are therefore

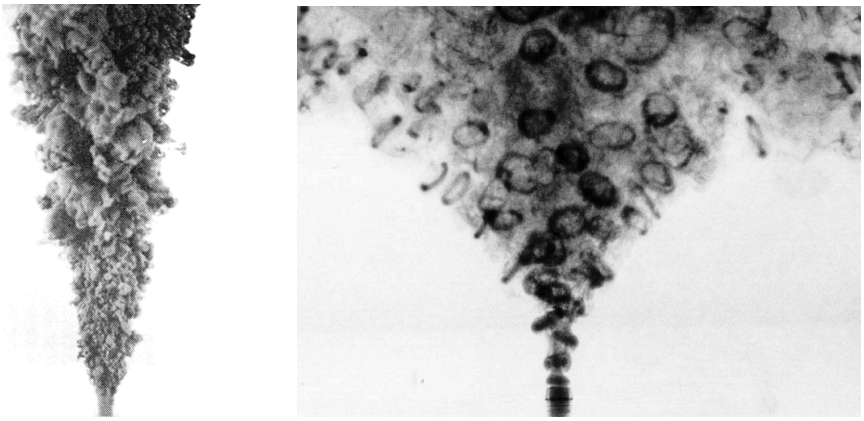

FIGURE 7.12. The left figure is a normal circular jet without forcing. The 'blooming' jet on the right was obtained by slightly wobbling and pulsing the exit nozzle of a circular jet in water (Lee & Reynolds 1985). The perturbation excites a Kelvin-Helmholtz-type intrinsic instability, as in the perturbed shear layer in figure 7.9.

responsible for the growth of the layer, and if they in turn originate from the amplification of small initial perturbations, it should be possible to control the characteristics of the layer by manipulating the initial conditions.

One example is shown in figure 7.12. On the left is a regular jet coming out from a circular nozzle, visualized by the addition of a dye to the nozzle fluid. In the same way that plane shear layers are subject to the Kelvin–Helmholtz instability and roll into discrete spanwise vortex lines, jets can be modelled as trains or vortex rings which grow from the instability of the cylindrical vortex layer that separates the fast fluid in the nozzle from the quiescent one outside. Vortex rings are subject to pairing instability, as in the case of two-dimensional vortex lines, and eventually the ordered array of rings coming out from the nozzle becomes disorganized as the jet spreads. As in the case of shear layers this disorganization can be promoted by injecting perturbations at the nozzle, and this effect can be used to control the growth of the jet. This is what was done in the experimental 'blooming' jet on the right-hand side of figure 7.12, in which the perturbation was introduced by slightly oscillating the exit nozzle at the same time as the stream was pulsed to promote the formation of the vortex rings. The difference in the growth rates of both jets is entirely due to the forcing. The growth rate of turbulent round jets is otherwise essentially universal.

There are several important differences between circular jets and plane layers. The main one is probably the energy carried by the blooming vortices. We saw in chapter 2 that it takes energy to separate two-dimensional vortices of the same sign, because the velocity of the fluid in the region between the vortices decreases as they separate. That is the reason why it was impossible in the forced shear layer in figure 7.9 to increase the growth rate for more than a finite length. Spreading the layer separates its vortices, and the growth rate eventually has to go back to its natural value which, as we saw at the beginning of this chapter, is controlled by the turbulent energy-dissipation rate.

Pairs of vortices of opposite signs are different. They contain little energy, because they have no net circulation when seen from far away, and therefore induce only weak velocities even when seen from a distance of only a few times their separation. While moving apart

two equal vortices by an infinite distance changes their energy by an infinite amount, doing the same thing with two vortex dipoles takes only a finite energy expenditure. The same is true of vortex rings in three dimensions, which also carry no net circulation, and the enhanced growth rate of jets such as the one in figure 7.12 can be maintained indefinitely without changing their dissipation rate too much. A survey of jet manipulation schemes and of their applications can be found in (Reynolds *et al.* 2003).

In general, and although aspects such as the influence of compressibility, of density differences, and of the three-dimensionality of the mean flow, are still subjects of active research, free shear flows are amongst the best understood, and most easily controlled, turbulent flows.

Problem 7.9: Use the expression for the energy of a vortex system given in equation (2.51) in chapter 2 to show that separating two vortices of circulation γ, initially at a distance D_0 from each other, to a distance D releases an energy of the order of $\gamma^2 \log D/D_0$.

Show next that separating from each other two vortex dipoles, each of which is formed by vortices of circulation $\pm\gamma$ separated by a distance a, takes only a finite energy of the order of $\gamma^2 a^2/D_0^2$.

7.4 Shear sheltering

An aspect of shear flows that is interesting enough to be studied separately is the effect of ambient turbulence on an isolated shear layer. This is for example important when considering whether turbulence in the free stream modifies transition in a laminar boundary layer, or in other shear flows, or whether localized shear could act as a barrier to perturbations present on one of its sides. Consider a convex corner velocity profile like the one in figure 7.5(*b*), separating a uniform stream $U = U_0$ at $x_2 > 0$ from a constant positive shear $U = U_0 + Sx_2$ at $x_2 < 0$. Rayleigh's equation for the vorticity perturbations in each of the two streams becomes

$$(U - c)\widehat{\Phi} = 0, \tag{7.89}$$

and can either be satisfied by $c = U_0$, in which case $\widehat{\Phi}$ is arbitrary for $x_2 \geq 0$, or by $\widehat{\Phi} = 0$. This implies that vorticity waves can exist in the upper stream, where they are neutrally stable and are advected by the uniform mean velocity, but that they can not penetrate into the shear. This is the long-term limit of the effect of shear on pre-existing turbulence, that we already saw in section §7.2.3 to be that the large scales are deformed into narrow sheets, and dissipate either nonlinearly or by the effect of viscosity. In the present non-homogeneous case the effect is still more striking.

Assume that $\widehat{\Phi} = \widehat{\Phi}_T(x_2)$ in the uniform stream, determined by the initial conditions. The wall-normal velocity satisfies Laplace's equation (7.56), and can be written in terms of some particular solution $\widehat{u}_{2T}$ and of a corner wave. The solution in the shear layer is irrotational and only contains the corner wave,

$$\widehat{u}_2 = \begin{cases} \widehat{u}_{2T}(x_2) + [A_T - \widehat{u}_{2T}(0)]\exp(-\overline{\kappa}x_2), & x_2 \geq 0, \\ A_T \exp(\overline{\kappa}x_2), & x_2 \leq 0. \end{cases} \tag{7.90}$$

Its intensity is given by the jump condition (7.64),

$$A_T = \frac{U_0 - c}{2\overline{\kappa}(c_0 - c)} \left(\frac{\mathrm{d}\widehat{u}_{2T}}{\mathrm{d}x_2}(0) + \overline{\kappa}\widehat{u}_{2T}(0) \right) \tag{7.91}$$

where $c_0 = U_0 - S/2\overline{\kappa}$ is the phase velocity (7.65) of a corner wave with wavenumber $\overline{\kappa}$.

The interesting effect appears when the perturbation in the free stream moves with a phase speed $c = U_0$, as in the linear case. The jump condition then reduces to $\widehat{u}_2(0) = A_T = 0$, and

$$\widehat{u}_2 = \begin{cases} \widehat{u}_{2T}(x_2) - \widehat{u}_{2T}(0)\exp(-\overline{\kappa}x_2), & x_2 \geq 0, \\ 0, & x_2 \leq 0. \end{cases} \tag{7.92}$$

Thus not only is the vorticity of the free-stream turbulence excluded from the shear layer, but even the potential pressure perturbations that it induces are blocked by a vorticity corner wave that exactly cancels them. This 'shear-sheltering' effect was first recognized by Hunt & Carruthers (1990), and has for example been invoked to explain the appearance of diffusion barriers across steep meridional gradients of the stratospheric winds, such as in the containment of ozone depletion within the circumpolar vortex, and in the damping of turbulence in some plasmas. We have already mentioned its possible role in limiting the triggering of early transition in boundary layers by outside turbulence.

Another interesting interpretation is that the decay of two-dimensional turbulence to a few isolated vortices, which was discussed in chapter 2, is also a manifestation of shear-sheltering. Once a strong vortex has been established by, for example, merging of smaller ones, it protects itself from the remaining background turbulence by its self-induced internal shear. The vortices thus become drops of essentially laminar fluid in the turbulent flow. A survey of situations in which shear sheltering is important, with special emphasis on plasma turbulence, is given by Terry (2000).

It follows from (7.91) that blocking is only one of the possible outcomes of the interaction of a localized shear layer with potential waves originating from the free stream. In real flows the advection velocity of vorticity is not always the same as that of the ambient fluid. Groups of interacting vortices move with respect to the flow. Think for example of the case of a second shear layer, or of a jet in the neighbourhood of the corner in the previous example. The amplitude in (7.91) even becomes infinite if the phase velocity of the perturbations coincides with the natural velocity of a corner wave of the same wavenumber. No steady solution is possible in that case. If the outside forcing is treated as given, the corner wave grows linearly in time, and it is even possible for it to resonate with the forcing perturbation, so that the global flow becomes unstable. We saw in section §7.2.3 that such resonances are at the root of many inviscid instabilities. In general, except for the particular case in which $c = U_0$, external vorticity is prevented from entering into a vorticity layer, but potential perturbations penetrate distances of order $\lambda = 2\pi/\overline{\kappa}$, with amplitudes that are proportional to $|c - U_0|$.

When the profile is smoother than a simple corner, the sheltering effect extends to a range of phase velocities. The reader may like to prove as an exercise that, for a piecewise-linear profile joining a uniform stream with a constant shear, perturbations from the former are blocked away from the latter whenever their phase speed coincides with the fluid velocity at any of the corners of the profile.

Inspection of the full Rayleigh's equation,

$$(U - c)\widehat{\Phi} - U''\widehat{u}_2 = 0, \tag{7.93}$$

reveals the underlying problem. Whenever $U = c$, the coefficient of the highest-order term vanishes, and the equation is locally singular. At those 'critical layers' $\widehat{u}_2$ has to vanish

unless the curvature of the profile is also locally zero, $U'' = 0$, and they form rigid barriers that neutral perturbations cannot cross.

In the typically-unstable free shear flows critical layers do not exist, because the phase velocities are complex, but they are key features in the wall-bounded flows studied in the next chapter, and in other cases that are either neutral or very weakly stable or unstable. The perturbations then accumulate near the critical layer, and the fluctuating velocities above and below it behave largely independently of each other.

A serious study of critical layers is beyond our scope, and the reader is encouraged to look for more information in any of the stability textbooks mentioned above. They are important because it is there that the usual assumptions for the evolution of the vorticity cease to hold. The vorticity perturbations are created when u_2 deforms transversely the mean shear. Vorticity then moves away from the forcing because it is advected by the mean velocity U. When the mean velocity locally coincides with the phase velocity of the forcing, vorticity cannot be carried away, and accumulates. No steady state is possible until viscosity or nonlinearity take over, and the critical layers cannot be treated correctly unless one or the other are taken locally into account. The real reason why we have used piecewise-linear profiles in the examples in this chapter has been to avoid the complications of dealing with critical layers.

Shear sheltering is the particular case in which the phase velocity of the perturbations is such that the critical layer is located at the edge of the shear. The viscous case has been analyzed by Jacobs & Durbin (1998). The penetration length of the external vorticity is then of the order of $(\nu\lambda_1/S)^{1/3}$, where λ_1 is the streamwise wavelength. This thickness is typical of viscous critical layers.

The viscous penetration length vanishes in the limit $\nu \to 0$, in agreement with the inviscid analysis, but it becomes infinite when $\kappa_1 \to 0$, independently of the value of $\overline{\kappa}$. As always when dealing with parallel shear flows, the case $\kappa_1 = 0$ is special. The vortical structures are then infinitely long in the streamwise direction, and we saw in section §7.2.1 that the flow in the plane $(x_2 - x_3)$ decouples from the shear. In the linear approximation that implies that

$$\partial_t \widetilde{u}_2 = \partial_t \widetilde{u}_3 = 0. \tag{7.94}$$

The streamwise velocity acts as an advected passive scalar, and the fluctuations in $\widetilde{u}_1$ grow algebraically in time at the expense of the mean velocity profile. Equation (7.45) does not depend on the assumption that the shear is constant, and results in the formation of ever stronger 'streaks' as long as the linear approximation holds,

$$\widetilde{u}_1(t) - \widetilde{u}_1(0) = \widetilde{u}_2 U' t \tag{7.95}$$

In this case, as in those in which the phase velocity of the forcing is very different from that of the free stream, sheltering fails, and transition or turbulence within the shear layer can be forced by outside perturbations.